

Thermo-elastic induced phase noise in the LISA Pathfinder spacecraft

F Gibert¹, M Nofrarias¹, N Karnesis¹, L Gesa¹, V Martín¹,
I Mateos¹, A Lobo^{1‡}, R Flatscher², D Gerardi²,
J Burkhardt², R Gerndt², F Guzmán³, J Reiche³, G Heinzl³,
K Danzmann³

¹ Institut de Ciències de l'Espai (ICE-CSIC/IEEC), Barcelona, Spain

² Astrium GmbH, Friedrichshafen, Germany

³ Max-Planck-Institut für Gravitationsphysik, Hannover, Germany

E-mail: gibert@ieec.cat

Abstract. During the On-Station Thermal Test campaign of the LISA Pathfinder the data and diagnostics subsystem was tested in nearly space conditions for the first time after integration in the satellite. The results showed the compliance of the temperature measurement system, obtaining temperature noise around $10^{-4} \text{ K Hz}^{-1/2}$ in the frequency band of 1–30 mHz. In addition, controlled injection of heat signals to the suspension struts anchoring the LISA Technology Package (LTP) Core Assembly to the satellite structure allowed to experimentally estimate for the first time the phase noise contribution through thermo-elastic distortion of the LTP interferometer, the satellite's main instrument. Such contribution was found to be at $10^{-12} \text{ m Hz}^{-1/2}$, a factor of 30 below the measured noise at the lower end of the measurement bandwidth (1 mHz).

1. Introduction

LISA Pathfinder (LPF) [1] will be the in-flight experiment to test key elements required for a future space-borne gravitational wave detector, as the proposed eLISA [2]. LPF is an ESA mission, with some NASA contributions [3]. The main scientific instrument on-board the LPF is the LISA Technology Package (LTP), consisting of two test masses which are kept in nominal free fall by means of a precise drag-free control loop [5]. A high precision interferometer [4] measures the relative longitudinal and angular displacements with high stability, i.e. down to 1 mHz.

The main scientific goal of the mission is to reach a residual acceleration between both test masses of $3 \times 10^{-14} \text{ m/s}^2/\sqrt{\text{Hz}}$ down to 1 mHz [6], as expressed in amplitude spectral density of differential acceleration fluctuations between them. Under these conditions of extremely low residual acceleration, several environmental noise sources could induce disturbances in the system that would reduce the sensitivity of the system, if they are not antecedently accounted for. The Diagnostics Subsystem on-board LISA Pathfinder is designed precisely for that purpose: it will monitor magnetic fields [7], charged particles [8] and temperature variations on the satellite [9]. It also includes a set of precision heaters and coils that will allow a characterisation of the effects in-flight and its consequent translation into noise models to be taken into account for any future gravitational wave observatory in space.

The thermal case is of particular relevance since it becomes more important in the very low frequency regime, where LISA Pathfinder has its measurement bandwidth. Also, thermal effects have been identified as a leading term in the noise contribution through different effects, namely: net forces and torques appearing on the test masses caused by asymmetric temperature distributions around them, optical path-length variation due temperature fluctuation of optical elements and thermo-elastic distortion of the satellite structure, including the distortion of the Optical Metrology Subsystem's optical bench itself. While there have been experiments addressing the first two —through torsion pendulum measurements [10] and laser metrology set-ups [11], respectively— there were no empirical results providing an indication of the impact of the temperature-induced deformation of the structure hosting an instrument as the LTP, reaching picometer resolution.

Spacecraft thermal-vacuum tests are the first realistic scenario where these experiments can take place. In the following we describe the LISA Pathfinder On-Station Thermal Test (OSTT) campaign which took place late in 2011, involving for the first time thermal diagnostics experiments to be carried out during the mission and providing critical information regarding the LTP sensitivity towards thermoelastic perturbations at the LTP Core Assembly (LCA).

The paper is organized as follows. We describe the set-up during the campaign and the experiments performed in Section 2. Results on the thermo-elastic noise contribution to the optical metrology are presented in Section 3, to then finally discuss our conclusions in Section 4.

2. The LISA Pathfinder Thermal Balance and Thermal Vacuum campaign

Thermal Balance and Thermal Vacuum test are one of the most comprehensive series of test that a spacecraft needs to overcome before launch. The main purpose of the Thermal Vacuum test is to verify the satellite performance in its thermal design limits. This set of thermal data is required as well for correlation with the spacecraft thermal model. On the other side, Thermal Balance checks the performance of the spacecraft by operating all of its systems in the same simulated space conditions until thermal equilibrium is achieved.

For LISA Pathfinder, these represented an extensive campaign of tests conducted at the IABG mbH space simulator, in Ottobrun (Germany) –see Figure 1. During the campaign, the spacecraft was operated in space conditions, i.e. with a nominal pressure below 10^{-4} Pa and powered up by means of a sun simulator, consisting of an array of high power lamps mimicking the radiation that will hit the spacecraft in orbit.

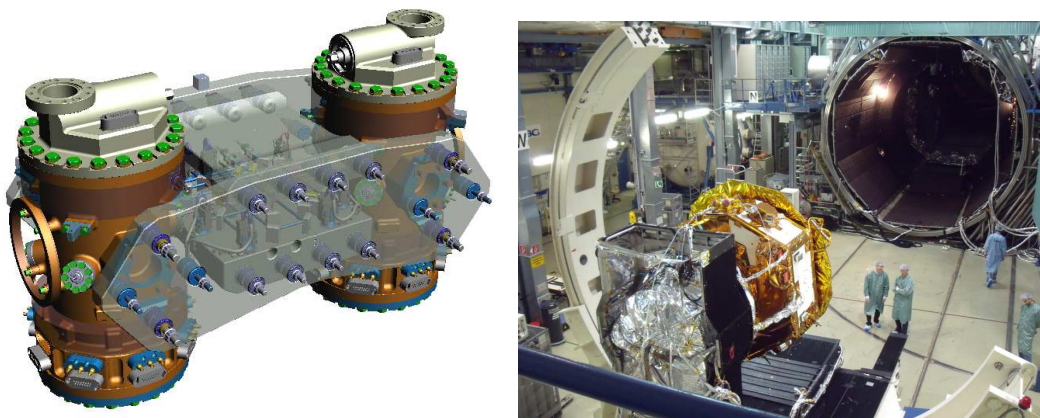


Figure 1. *Left:* General view of the LTP Core Assembly (LCA), with both Vacuum Enclosures that host the Inertial Sensors. The optical bench is located between them. Image credits: Astrium, Germany. *Right:* IABG mbH space vacuum chamber with the LISA Pathfinder during the OSTT campaign. Image credits: Astrium UK.

The instrument on-board the satellite was almost the complete flight version of the LISA Pathfinder satellite. Most parts of the different satellite units were already integrated and operative. However, though the LISA Pathfinder optical metrology was already fully operative, the Electrode Housings and the test masses of the Inertial Sensors were not yet present and were replaced by piezoelectric driven mirrors acting as end-mirrors of the interferometer [12].

Such changes directly affected the layout of the different diagnostics items. Regarding the temperature sensors, 8 thermistors were relocated around the dummy Inertial Sensor Housing structures and 6 placed on the inner sides of the LCA support structure, leaving at their flight representative locations only the 6 Suspension Struts temperature sensors and the 4 sensors located on the optical bench —see Figure 2. Despite of the modifications, the temperature measurement subsystem could perform

correctly. About the heaters, only the 6 Suspension Strut heaters were present and placed in their *design* location. As a consequence, among the different heating experiments planned for mission, only the thermistors and heaters concerning the Suspension Strut heating were available for test.

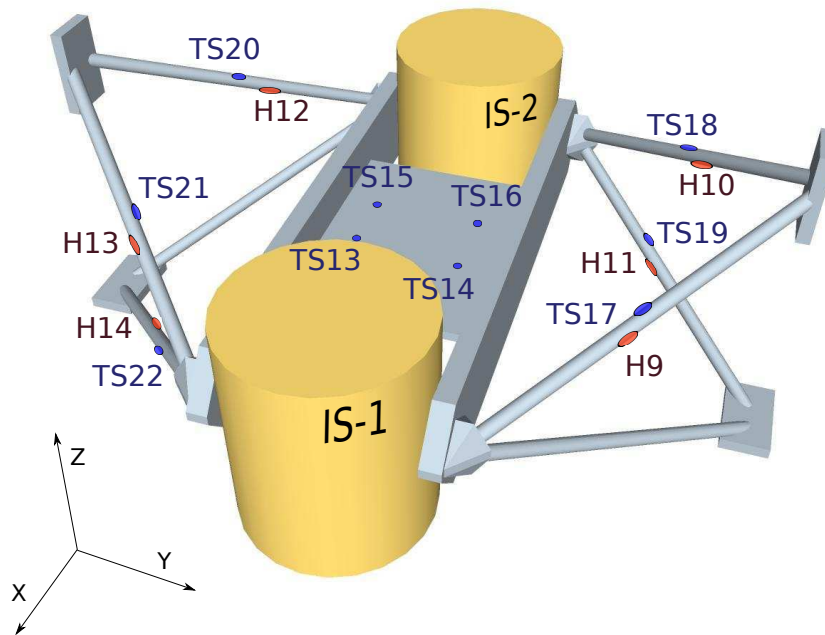


Figure 2. Scheme of the LCA and its series of diagnostics heaters and temperature sensors on the different Suspension Struts and on the optical bench, as during the OSTT campaign.

2.1. Thermal Diagnostics experiments during the campaign

The campaign was divided in two main stages, where experiments involving many different subsystems of the spacecraft were repeated at two different temperatures, i.e. the *hot case* at $30.5^{\circ}\text{C} \pm 0.5^{\circ}\text{C}$ and the *cold case* at $9.5^{\circ}\text{C} \pm 0.5^{\circ}\text{C}$, reaching temperatures of around 26°C and 12°C respectively in the LCA [12]. In both of them series of experiments to test system performance and to characterise different spacecraft subsystems were run and, as regards of the thermal diagnostics, the execution of different telecommand sequences of heater activations was included. These experiments were carried out during the *cold case* and were planned as follows:

- Phase 1: Continuous heat injection in Heaters 9 and 11 (14h).
- Phase 2: Individual heater activations in series of pulses to all strut heaters ($6 \times 2\text{h}$).
- Phase 3: Combined heater activation for thermoelastic stress tests (10h).
- Phase 4: Relaxation time (12h).

Phase 1 experiment is aimed to test long-term heating system performance while *Phase 2* experiments are providing most of the information regarding the system response to local —at a single *Suspension Strut level*— temperature fluctuation. The incidence of such experiments to the interferometer readout is expected to be linear, what is checked with data from *Phase 3*. *Phase 4* is providing with a set of noise data where to analyse the amount of temperature noise contribution during normal performance of the system as well as with information regarding the relaxation times needed to recover from heater-induced conditions.

The whole data communication chain between the spacecraft and the operations center was already through the flight model [8] and OBC (On-Board Computer), and the spacecraft kept being powered up from the solar-like radiation energy provided by an array of high power lamps in the vacuum chamber.

2.2. Temperature environment characterisation

The temperature measurement subsystem kept active through all the tests of the campaign, allowing a complete characterisation of the environment whilst the different planned experiments were taking place. Before entering in the analysis of the measurements obtained through the set of temperature sensors, it is worth describing the temperature acquisition readout and the associated data pre-processing.

The LPF temperature measurement system is based on series of Wheatstone bridges centred at different temperatures in order to perform all the measurements close to the linearity of the system, what ends up composing the total temperature range [13]. However, the transition between different ranges (or *scales*) is not perfectly smooth and residual offset jumps may appear. In addition, due to limitation on the downlink telemetry budget for diagnostics, the measured data at 0.83 Hz is on-board downsampled to 0.21 Hz with a Butterworth filter before being transmitted. As a consequence of the previous, spikes can appear along the data at each change of scale —related with a change of the reference resistor used at the Wheatstone bridge. In order to clean the signal from such spikes, sets of samples are removed and interpolated, while the remaining offsets are carefully identified and subtracted.

On the other side, the interferometer data is received at 10 Hz and it is providing mainly the following measurements: the relative displacement between the end-mirrors acting as *dummy* test masses (x_{12}), the displacement between the end-mirror at +X test mass location and the spacecraft (x_1), and four angles regarding the Y and Z inclination of each test mass —end-mirrors during the test campaign. This data is resampled to 0.21 Hz and interpolated to the same timing grid of the temperature sensors. This operation is mandatory in order to compute the transfer functions in Section 3.

All the data treatment and analysis have been carried out with software from the LISA Technology Package Data Analysis (LTPDA) toolbox, which is a dedicated MATLAB Toolbox developed by the LPF Data Analysis team, integrating the different data analysis tools to be used during the mission and the posterior data analysis

phase [14].

The measurements obtained during the campaign show a measured performance below the $10^{-4} \text{K Hz}^{-1/2}$ for frequencies higher than 2 mHz in the optical bench —see Figure 3. Some extra noise in the low frequencies was attributed to temperature noise in the environment. The best stability was found on some *relocated* sensors outside the LCA, achieving a noise level of $10^{-5} \text{K Hz}^{-1/2}$ through most frequency band, in practice achieving the electronic noise floor, as expressed by the *reference* measurements (i.e. measurements performed with high stability resistors). Such low levels were not achieved inside the LCA because of a high temperature drift that induced a beatnote in the temperature readout through an already identified analog-to-digital converter *non-linear* error [15]. Such a high temperature drift appeared due to test schedule limitations, i.e. not allowing the instrument to achieve a complete steady state. The real drift during flight operations is thus expected to be smaller. Appendix A focuses on this particular issue, and how the error coming from the thermal drift is identified.

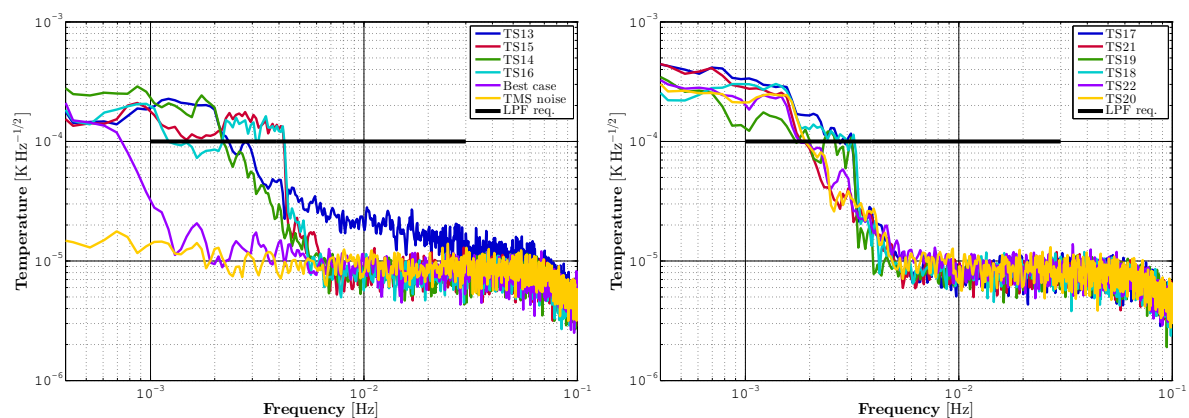


Figure 3. *Left:* Power Spectral Density (PSD) for the optical bench temperature sensors, together with the best performance case of the temperature measurement subsystem (TMS), obtained outside the LCA by a *relocated* sensor and the system reference noise, which sets the floor for the temperature measurement. *Right:* PSD of the different Strut temperature sensors. The bumps followed by sudden noise falls in the middle of the bandwidth are attributed to non-linear effects of the ADC, caused by the presence of too high temperature drifts during the campaign— see Appendix A.

3. Thermo-elastic contribution to phase noise

During the *Phase 2* of the diagnostics experiments within the campaign, a series of three pulses of 200 s in periods of 1000 s and an amplitude of 2 W were applied individually to each heater, producing temperature increments in the local strut around 8 K per pulse what induces immediate observable consequences on the interferometer channels with amplitudes around $\pm 5 \text{ nm}$, as shown in Figure 4. In order to better distinguish the effect, a 1st-order detrend is applied to all time series in the Figure 4.

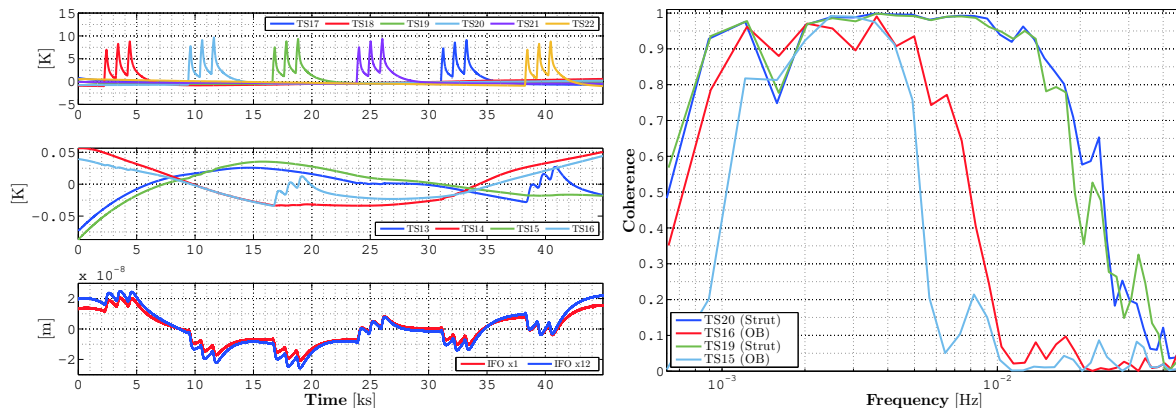


Figure 4. On the *left* side, the temperature measurements at the different struts (*upper* plot), the optical bench temperatures (*centre* plot) and the displacements measured by the interferometer (IFO, *lower* plot), all of them detrended with a 1st-order polynomial. On the *right*: coherences between different strut sensors (TS19 and TS20) and interferometer’s channel x_{12} together with the coherences from their closest optical bench (OB) sensors (TS15 and TS16 respectively) to the same interferometer measurement.

Temperature increments at the optical bench clearly indicate that temperature variations in the lower struts (TS19, TS22) have a thermal impact on the optical bench much larger than the upper struts (TS17, TS18, TS20, TS21). Indeed, the central panel in Figure 4 shows how the temperature sensors in the optical bench have a clear response for the former and a negligible reaction —out of the environmental drift— for the latter. An explanation of this effect must be sought in the fact that, opposite to the upper (+Z) struts —see Figure 2—, the screws attaching the lower (-Z) struts to the optical bench assembly present direct visibility to their closest optical bench sensor, establishing a direct thermal radiative link. If we consider the screw temperature being increased 1 – 2 K through thermal conduction, similar to what has been measured in lab, increments of some tenths of K should be expected in these optical bench sensors, about one order of magnitude above the equivalent case with just conduction —which is the case for the higher struts.

Nevertheless, the lower left hand plot in Figure 4 shows how the interferometer perturbation repeats the same pattern of signals for all the heater activations, regardless of the above discussed asymmetry on +Z and -Z struts. In order to further investigate this effect, we computed the coherence function between the interferometer phase readout and the four temperature sensors involved in the -Z struts experiments. As shown in Figure 4 (*right*), the analysis confirms that the signal observed in the interferometer is not coherent with temperature variations observed in the optical bench ($\simeq 8\%$ coherence 10 mHz with sensors TS15 and TS16) and is strongly correlated with the temperature increase in the struts ($\simeq 92\%$ coherence at 10 mHz with sensors TS19 and TS20). This suggests that, though the Zerodur plate is being heated up through radiative effects when activating lower-strut heaters, the interferometer

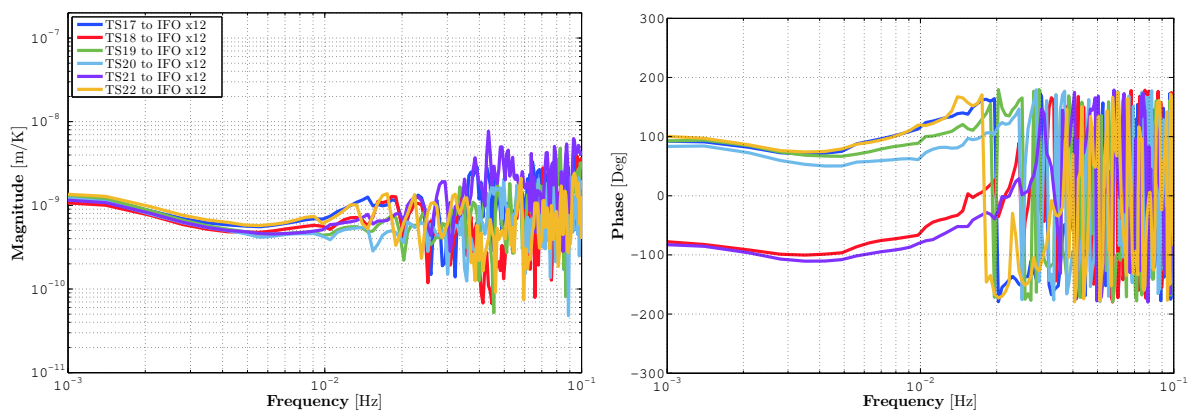


Figure 5. Transfer functions from the temperatures at the suspension struts to displacement as measured by the interferometer measuring the distance between both test masses (x_{12}), magnitude (*left*) and phase (*right*).

sensitivity in front of this effect is negligible in comparison to the general strut heating effect, discarding the Zerodur plate heating up as the mechanism describing the main perturbation and pointing to a global elastic distortion effect on the LCA.

Once the origin of interferometer response has been traced, we can proceed to quantify its contribution to the noise budget. We start by computing the individual transfer functions from the the temperature signals to the interferometer readouts, given by [16]

$$H_{T_i\Phi}(\omega) = \frac{S_{T_i\Phi}(\omega)}{S_{T_iT_i}(\omega)} \quad (1)$$

where T_i and Φ are the Suspension Strut temperature sensor and the interferometer signals respectively, and $S_{T_i\Phi}(\omega)$ and $S_{T_iT_i}(\omega)$ are the cross-power spectral density and the power spectral density. The transfer functions for each strut is shown in Figure 5. The thermo-elastic coupling of the struts to the interferometer is of 10^{-9} m/K throughout most of the LTP band. No significant differences between transfer functions are found since the geometry of the LCA is symmetric regarding all the suspension struts and the interferometer. The noise at frequencies higher than 70 mHz correspond to the band where the ambient noise is lower than the electronic noise and the signals become uncorrelated.

The system linearity in front this distortion is checked by comparing such transfer functions with respect to data from *Phase 3*. In this phase 500s pulses are applied simultaneously to TS17 and TS19 alternating with pulses to TS20 and TS22, producing a 2 mHz perturbation signal to the interferometer. The transfer function from the addition of all the former involved temperature sensors to each interferometer channel match with the contribution computed separately (10^{-9} m/K for the case of x_{12}), meaning that, as expected, the thermoelastic strain mechanism keeps within its linearity.

Following the previous notation, the thermo-elastic phase noise contribution to the

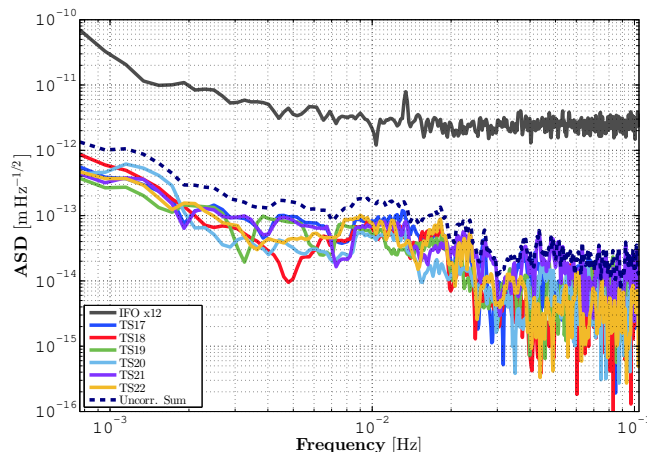


Figure 6. Noise projection of thermo-elastic induced phase noise on the interferometer x_{12} . The contribution from each suspension strut is shown together with the uncorrelated sum of all.

total interferometer noise –known also as *noise projection*– can be obtained by

$$S_{\Phi\Phi, T_i}(\omega) = H_{T_i\Phi}(\omega)S_{T_i T_i}(\omega) \quad (2)$$

where to evaluate $S_{T_i T_i}(\omega)$ we now use a segment without heat injections, as the ones shown in Figure 3. The results —in Figure 6— show how the overall thermo-elastic phase noise contribution accounts approximately for 10^{-12} m/ $\sqrt{\text{Hz}}$ at 1 mHz, assuming that all contributions are added in an uncorrelated sum. No differences are appreciated between contributions to the different interferometer readouts and also between the hot case and the cold case.

It is worth stressing that the obtained contribution is not representative of the flight operations since temperature stability is expected to be better in the Lagrange point L1 compared to the current experiment. However, the analysis reported here will be valid for the mission analysis.

4. Conclusions

We have presented first results for the thermal diagnostics sensors on the LISA Pathfinder spacecraft in space-like conditions. During the campaign, the temperature measuring system achieved an in-band sensitivity of 10^{-4} K Hz $^{-1/2}$ in those parts not exposed to temperature drifts higher than 10^{-5} K/s. The electronic of the measurement subsystem kept the noise floor down to 10^{-5} K Hz $^{-1/2}$. Among other thermal experiments, a set of heat injections were applied at each Suspension Strut anchoring the LTP Core Assembly at the satellite’s mechanical support structure for the LTP, which is acting as well as thermal shield. This temperature modulation allowed us, for the first time, to experimentally determine the coupling of temperature fluctuations on the struts to the interferometer onboard. We have estimated a nearly flat transfer function throughout the measuring bandwidth with magnitude 10^{-9} m/K.

At the same time, we have allocated the contribution arising from temperature fluctuations in the struts to be 10^{-12} m/ $\sqrt{\text{Hz}}$ at 1 mHz, around a factor 30 below the main interferometer measurement floor noise, for the campaign conditions (which in turn was a factor of approximately 3 better than required for flight). Although the obtained results are related to the particular temperature environment of the campaign, the methodology described here is readily applicable to the in-flight case.

We have also investigated the origin of the coupling between temperature fluctuations and interferometer response to conclude that the effect has a thermo-elastic origin, discarding direct temperature gradients on the optical bench as the cause of the observed phase response.

Coupling through other thermal sensitive locations, as for instance the electrode housing surrounding the test mass can be disregarded since they were not present in the current setup. The temperature-induced pathlength variation at the Optical Window [11] has not been assessed since, though the Optical Windows were present in the setup in a thermally almost representative mount with respect to the optical bench, no mission-planned experiments were performed on them. These effects, which will be the aim of the thermal experiment during flight operations, are being end-to-end simulated [17] and tested on-ground through other setups [10, 11].

Appendix A. Identification and fit of the ADC non-linear error

The bumps that appear in the power spectra of some temperature sensors, in the LPF band –see Figures 3, *left*–, are individually associated to integral non-linearities of specific bits of the 16-bit Analog-to-Digital Converter (ADC). Their affected frequencies depend on the signal drift. Each bit contribution –as a voltage error– is frequency-dependent and it can be expressed as [15, 18]:

$$|q_k(\omega)| = \Delta \sum_{n=-\infty}^{\infty} \frac{\sin \frac{n\pi\epsilon_k}{2^{k+1}\Delta}}{n} \frac{\sin \frac{n\pi}{2}}{\sin \frac{n\pi}{2^{k+1}}} \delta \left(\omega - \frac{\pi n |b|}{2^k \Delta} \right) \quad (\text{A.1})$$

where:

- b is the temperature slope, in K/s.
- Δ is the ADC quantization step in V.
- k is the binary digit, increasing from 0 to 15, i.e. from the least significant bit to the most significant.
- ϵ_k is the relative error associated to each bit, as a fraction of Δ .

In the case at Figure A1 the affected frequencies clearly oscillate close to 3 mHz and 6 mHz, which is consistent with a bit mismatch at the 2nd and 3rd LSB bit of the ADC in front of a mean drift of 6 $\mu\text{K/s}$, considering a system sensitivity of 1.35 K/V. The noise level introduced, around 2×10^{-4} K Hz^{-1/2}, clearly exceeds the ambient level by a factor two.

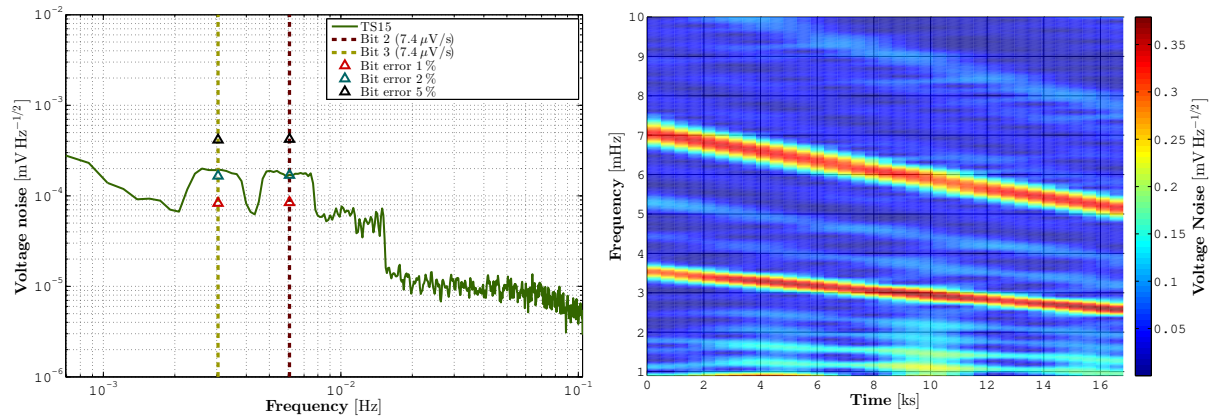


Figure A1. *Left:* PSD of the noise at TS15 at specific segment where the ADC non-linear effects create two bumps around 3 mHz and 6 mHz caused by bit errors at bits 2 and 3 in form of a voltage drift of $7.4 \mu\text{V/s}$. *Right:* Spectrogram of the voltage during chosen segment. The reddish lines show the affected frequencies varying within the time, caused by the variation of temperature drift.

Limits to the temperature drift can be obtained from these analysis. Since the bumps noise amplitude of this error depend only on the Δ parameter which cannot be modified, the highest-frequency bump must be shifted down, out of the bandwidth of interest. In this sense, in order to reduce its highest frequency affected (8 mHz) to 1 mHz, the temperature drift must be therefore limited to 1/8 of the measured, around $7.5 \mu\text{K/s}$.

Acknowledgements

The authors acknowledge support from Project AYA2010-15709 of *Plan Nacional del Espacio* of the Spanish Ministry of Science and Innovation (MICINN) and support by Deutsches Zentrum für Luft- und Raumfahrt (DLR) with funding of the Bundesministerium für Wirtschaft und Technologie project reference No 500Q0501. Astrium GmbH, Friedrichshafen, Germany, planned and conducted the LTP thermal experiments based on ICE-CSIC/IEEC plans and provided the test data obtained at occasion of the LISA Pathfinder Spacecraft On-Station Thermal Test. This thermal test was conducted by Astrium UK as the spacecraft responsible. ESA supported by several national space agencies is responsible for the entire LISA Pathfinder program. MN acknowledges a JAE-DOC contract from CSIC (co-funded by the ESF) and support from the EU Marie Curie CIG 322288.

References

- [1] McNamara P *et al* 2013 The LISA Pathfinder Mission, *ASP Conference Series* **467**
- [2] Amaro-Seoane P *et al* 2013 The Gravitational Universe, *Document submitted to the European Space Agency for the L2/L3 selection of ESA's Cosmic Vision program*
- [3] ODonnell J *et al* 2004 The Space Technology 7 Disturbance Reduction System, ESA SP-548 105

- [4] Heinzl G *et al* 2004 The LTP interferometer and Phasemeter *Class. Quantum Grav.* **21** 581
- [5] Dolesi R *et al* 2003 Gravitational sensor for LISA and its technology demonstration mission *Class. Quantum Grav.* **20** S99
- [6] Vitale S *et al* 2005 Science Requirements and Top-Level Architecture Definition for the LISA Technology Package (LTP) on Board LISA Pathfinder (SMART2), *Science Requirement Document* LTPA-UTN-ScRD, Iss3-Rev1
- [7] Díaz-Aguiló M *et al* 2011 Neural network interpolation of the magnetic field for the LISA Pathfinder Diagnostics Subsystem, *Exper. Astron.* **30** 1-21
- [8] Cañizares P *et al* 2011 The LISA Pathfinder DMU and Radiation Monitor, *Class. Quantum Grav.* **28** 094004
- [9] Cañizares P *et al* 2008 The diagnostics subsystem on board LISA Pathfinder and LISA, *Class. Quantum Grav.* **26** 094005
- [10] Carbone L *et al* 2007, Thermal gradient-induced forces on geodetic reference masses for LISA, *Phys. Rev. D.* **76** 102003
- [11] Nofrarias M *et al* 2008 Thermal diagnostic of the Optical Window on board LISA Pathfinder *Class. Quantum Grav.* **24** 5103
- [12] Guzmán F *et al* 2013 LISA Technology Package Flight Hardware Test Campaign, *ASP Conference Series* **467**
- [13] Sanjuán J *et al* 2007 Thermal diagnostics frond-end electronics for LISA Pathfinder, *Rev. Sci. Instrum.* **78**(10) 104904
- [14] Hewitson M *et al* 2009 Data analysis for the LISA Technology Package, *Class. Quantum Grav.* **26** 094003
- [15] Sanjuán J *et al* 2010 ADC non-linear error corrections for low-noise temperature measurements in the LISA band, *J. Phys.: Conf. Ser.* **228** 012041
- [16] Bendat, J. S. and Piersol, A. G. 1993 Engineering Applications of Correlation and Spectral Analysis, John Wiley & Sons, Inc.
- [17] Gibert F *et al* 2012 State-space modelling for heater induced thermal effects on LISA Pathfinder's Test Masses, *J. Phys.: Conf. Ser.* **363** 012044
- [18] Wadgy M F 1996 Effect of Additive Dither on the Resolution of ADCs with Single-Bit or Multibit Errors *IEEE Trans. Instrum. Meas.* **45** 610